



Published in final edited form as:

Cancer Res. 2019 April 15; 79(8): 1831–1843. doi:10.1158/0008-5472.CAN-18-2636.

Spleen tyrosine kinase-mediated autophagy is required for epithelial-mesenchymal plasticity and metastasis in breast cancer

Aparna Shinde^{1,2}, Shana D. Hardy^{1,2}, Dongwook Kim^{1,2}, Saeed Salehin Akhand^{1,2}, Mohit Kumar Jolly⁸, Wen-Hung Wang^{1,2}, Joshua C. Anderson⁴, Ryan B. Khodadadi⁵, Wells S. Brown^{1,2}, Jason T. George^{3,6}, Sheng Liu^{2,7}, Jun Wan^{2,7}, Herbert Levine³, Christopher D. Willey⁴, Casey J. Krusemark^{1,2}, Robert L. Geahlen^{1,2}, and Michael K. Wendt^{1,2,*}

¹Department of Medicinal Chemistry and Molecular Pharmacology Purdue University, West Lafayette, IN 47907

²Purdue Center for Cancer Research, Purdue University, West Lafayette, IN 47907

³Center for Theoretical Biological Physics, Rice University, Houston, TX 77005

⁴Department of Radiation Oncology, University of Alabama, Birmingham, AL 35233

⁵Department of Graduate Medical Education, Mayo Clinic, Rochester, MN 55905

⁶Medical Science Training Program, Baylor College of Medicine, Houston, TX 77005

⁷Department of Medical and Molecular Genetics, Indiana University School of Medicine, Indianapolis, IN 46202

⁸Centre for BioSystems Science and Engineering, Indian Institute of Science, Bangalore, India 560012

Abstract

The ability of breast cancer cells to transiently transition between epithelial and mesenchymal states contributes to their metastatic potential. Therefore, driving tumor cells into a stable mesenchymal state, as opposed to complete tumor cell eradication, presents an opportunity to pharmacologically limit disease progression by promoting an asymptomatic state of dormancy. Here we compare a reversible model of epithelial-mesenchymal transition (EMT) induced by TGF- β to a stable mesenchymal phenotype induced by chronic exposure to the ErbB kinase inhibitor lapatinib. Only cells capable of returning to an epithelial phenotype resulted in skeletal metastasis. Gene expression analyses of the two mesenchymal states indicated similar transition expression profiles. A potentially downregulated gene in both datasets was spleen tyrosine kinase (SYK). In contrast to this similar diminution in mRNA, kinome analyses using a peptide array and DNA-conjugated peptide substrates showed a robust increase in SYK activity upon TGF- β -induced EMT only. SYK was present in cytoplasmic RNA processing depots known as P-bodies formed during the onset of EMT, and SYK activity was required for autophagy-mediated

*To whom correspondence should be addressed: Michael K. Wendt, Department of Medicinal Chemistry and Molecular Pharmacology, Purdue University, West Lafayette, IN 47907. Phone: 765-494-0860. mwendt@purdue.edu.

COI: The authors declare no potential conflicts of interest

clearance of P-bodies during mesenchymal-epithelial transition (MET). Genetic knockout of autophagy related 7 (ATG7) or pharmacological inhibition of SYK activity with fostamatinib, a clinically approved inhibitor of SYK, prevented P-body clearance and MET, inhibiting metastatic tumor outgrowth. Overall, the current study suggests assessment of SYK activity as a biomarker for metastatic disease and the use of fostamatinib as a means to stabilize the latency of disseminated tumor cells.

Precis:

Findings present inhibition of spleen tyrosine kinase as a therapeutic option to limit breast cancer metastasis by promoting systemic tumor dormancy.

Introduction

Primary tumor metastasis is the culmination of several sequential processes including local and systemic invasion, dissemination and outgrowth within a secondary organ (1). Numerous studies have linked the process of epithelial-mesenchymal transition (EMT) to local invasion and dissemination (2). Additional studies also link EMT to the acquisition of a stem-like phenotype (3). However, separate studies indicate that tumor cells with a stable mesenchymal phenotype are less efficient at overcoming systemic dormancy and completing the last step of metastasis (4). Recently, we used a HER2 transformation model of human mammary epithelial cells (HME2) to establish stable and reversible states of EMT induced by lapatinib and TGF- β , respectively (5). Using this approach, we were able to establish that a cytokine-induced EMT is sufficient to facilitate resistance to lapatinib. Herein, we used these model systems to address the hypothesis that epithelial-mesenchymal plasticity (EMP) is required for metastasis. Moreover, we identify spleen tyrosine kinase (SYK) as a critical molecular mediator of EMP.

SYK is part of the EMT core signature of mRNAs down-regulated in mammary epithelial cells when EMT is induced by TGF- β , the expression of EMT-inducing transcription factors, or by the depletion of E-cadherin (6). There is also evidence that SYK can directly influence phenotypic transitions in epithelial cells. For example, depleting SYK in MCF10A mammary epithelial cells and in pancreatic carcinoma cells promotes morphologic and phenotypic changes characteristic of EMT (7,8). Finally, epithelial-derived cancer cells that bear a constitutive mesenchymal phenotype silence SYK expression via hypermethylation of its promoter (9). These studies suggest that SYK may serve as a tumor suppressor. However, expression values can be misleading, particularly with regard to kinases whose level of expression may not be consistent with the activity of the enzyme. Furthermore, even antibody-based protein analyses require robust expression of enzymes to obtain reliable readouts with regard to the activation state of a kinase. To overcome these drawbacks, we utilized direct enzymatic activity detection assays using a peptide substrate microarray. We also employed a phosphorylation assay in which a substrate peptide is conjugated to DNA oligonucleotides, whereby quantitative readouts of phosphorylation are achieved via qPCR. This method presents a highly sensitive and quantitative means to determine kinase activity within a sample (10)(11).

To establish the mechanisms by which SYK modulates EMT, we have previously utilized a mass spectrometry approach to establish a list of substrate proteins (12). Among the substrates uniquely phosphorylated by SYK were several RNA-binding proteins. These included UPF1, LIMD1, EIF4ENIF1, CNOT2, LARP1, HNRNPK and DDX6. All of these proteins are known to localize in mRNA processing depots known as P-bodies (13,14). P-bodies are dynamic cytoplasmic foci that contain mRNAs, microRNAs, and mRNA-binding proteins involved in translation repression, mRNA degradation, and microRNA-mediated silencing. We recently established that P-bodies form during the onset of EMT and are removed during mesenchymal-epithelial transition (MET) by the process of autophagy (15). Similar to EMT, the role of autophagy in tumorigenesis is dynamic and highly context dependent. However, recent studies indicate that autophagy is critical for cancer cells to overcome the stresses associated with several processes of metastasis, including survival during dormancy (16)(17).

Overall, our results strongly support the conclusion that EMP facilitates metastasis. We present DNA-conjugated peptide substrate assays as a highly sensitive, robust means to identify aggressive breast cancers. Using this approach, we establish that SYK activity is required for autophagy-mediated clearance of P-bodies during MET. Finally, our data indicates that pharmacological inhibition of SYK could serve as a unique therapeutic approach to limit the metastatic progression of breast cancer, not through tumor cell eradication, but maintenance of disseminated cells in an asymptomatic state of dormancy.

Materials and Methods

Cell lines and reagents

The HEK293 and 4T1 cells were obtained from the ATCC while the HMLE cells were a kind gift from Sendurai Mani (MD Anderson Cancer Center). The 4T1 and HMLE cells were constructed to stably express firefly luciferase and HMLE cells were transformed via overexpression of HER2 (HME2). Construction of the HME2 cells and their mesenchymal variants via treatment with TGF- β or Lapatinib were described previously (5,18). Normal murine mammary gland (NMuMG) cells were purchased from the ATCC. All cells were validated for lack of mycoplasma contamination using the IDEXX Cell check and Impact III testing on July 24th, 2018.

Immunological assays

For the co-immunoprecipitation assay, HEK293T cells stably expressing GST-SYK and EGFP-DCP1A were lysed as described above. EGFP-DCP1A was immunoprecipitated from the soluble fraction using GFP-Trap agarose beads (Chromotek). Bound immune complexes were washed with lysis buffer and subjected to immunoblotting using antibodies against GST and GFP. In separate experiments, whole cell lysates were analyzed by immunoblot using the following antibodies; pSYK, SYK, ATG7, Zo1, Zeb1, Slug (Cell Signaling Technologies), Actin (Santa Cruz Biotechnologies) or β -tubulin (DSHB). Where indicated, cells were harvested by tyrpsinization and stained with antibodies specific for CD44 and CD24 (Biolegend). Differential staining for these markers was analyzed by flow cytometry.

RNA sequence analysis

Parental, HER2 transformed HMLE cells (HME2-parental), were treated every three days with TGF- β 1 (5 ng/ml) or lapatinb (1 μ M) for a period of 4 weeks to generate lapatinib resistant (LAPR) and post-TGF- β mesenchymal cell conditions (5). These cells were sorted for a CD44^{hi} phenotype (BioLegend) and total RNA was isolated using E.Z.N.A (Omega Bio-Tek). RNA sequencing was conducted using the Illumina HiSeq 2500 platform. These data have been deposited on the GEO database (GSE115255).

Kinomic analyses

Lysates from HME2 cell conditions indicated above, were analyzed on tyrosine chip (PTK) and serine-threonine chip (STK) arrays using 15ug (PTK) or 2ug (STK) of input material as per standard protocol. Three replicates of chip-paired samples were used and phosphorylation data was collected over multiple computer controlled kinetic pumping cycles, and exposure times (0,10,20,50,100,200ms) for each of the phosphorylatable substrates. Slopes of exposure values were calculated, log2 transformed and used for comparison. Raw image analysis was conducted using Evolve2, with comparative analysis done in BioNavigator v6.2 (PamGene, The Netherlands).

qPCR-based kinase assays

A peptide substrate-oligonucleotide conjugate was prepared, as previously described (10). Briefly, a selective SYK peptide substrate derived from phage display selections (19) (SYKtide, EDPDYEWPSA) was purchased from GenScript on Rink amide polystyrene resin, and the N-terminus was acylated with 5-hexynoic acid. Peptide was cleaved from resin by incubating in a cleavage cocktail (95:2.5:2.5 TFA:H₂O:TIPS) for 4 hours followed by a precipitation in cold ether. The resulting precipitate was subsequently purified by semi-prep HPLC at a flow rate of 5mL/min with H₂O (0.1% TFA) and MeCN (0.1% TFA) as mobile phase. The peptide was characterized by MALDI/MS. m/z: [M+H]⁺ calcd. for C₆₀H₇₇N₁₂O₂₁⁺, 1301.53, found [M+Na]⁺, 1323.35, [M+K]⁺, 1339.32.

The SYKtide alkyne was conjugated to a 20-mer DNA oligo (ATGGTATCAAGCTTGCCACA) containing a 5' azide modification, as described (11). The resulting conjugate was precipitated by adding 100 μ L of 10M ammonium acetate and 800 μ L of EtOH and being kept in -20°C overnight. After removal of supernatants, the resulting conjugate was purified by semi-prep HPLC at a flow rate of 1mL/min with H₂O (0.75% hexafluoroisopropanol (HFIP), 0.75% triethylamine (TEA), 5 μ M EDTA, pH 7.0) and 10:90 H₂O:MeOH (0.75% HFIP, 0.75%TEA, 5 μ M EDTA, pH 7.0) as mobile phase. The resulting conjugate was characterized by ESI/MS. m/z: [M-5H]⁵⁻, calcd. 1600.6, found 1600.7, [M-6H]⁶⁻, calcd. 1333.7, found 1333.7, [M-7H]⁷⁻, calcd. 1143.0, found 1142.8, [M-8H]⁸⁻, calcd. 1000.0, found 1000.0, [M-9H]⁹⁻, calcd. 888.8, found 888.8, [M-10H]¹⁰⁻, calcd. 799.8, found 799.8, [M-11H]¹¹⁻, calcd. 727.0, found 727.0, [M-12H]¹²⁻, calcd. 666.3, found 666.3, [M-13H]¹³⁻, calcd. 615.0, found 615.0.

MPER lysis buffer (Thermo Scientific 78501) was prepared with protease and phosphatase inhibitors (Protease Inhibitor Cocktail 1, Sigma #P8340, Phosphatase Inhibitor Cocktail 2, Sigma #P5726, and Phosphatase Inhibitor Cocktail 3, Sigma #P0044) at 1:100 concentration

each in our sample preparation. HME2 cell derivatives (1 million cells each) were harvested, treated with lysis buffer (500 μ L) to each cell pellet, and incubated on ice for 30 minutes. Cell lysate was obtained by centrifugation for 10 minutes at 4 °C at 14,000 g. The protein concentration was quantified using BCA protein assay solution (Thermo scientific).

Kinase activity reactions were performed in 50 mM Tris-HCl pH 7.5 and 10 mM $MgCl_2$, 1 mM ATP, 2 mM DTT, 1 μ M phagatide-DNA conjugate (20-mer DNA oligo), and 1 μ g total protein from cell lysates. Reactions were performed at room temperature for 30 minutes, and then enzymes were heat denatured by treatment at 65 °C for 5 minutes. After cooling to room temperature, encoding 55-mers were allowed to anneal for 30 minutes, as described (11). Selective purification of DNAs bearing phosphorylated peptides was performed using anti-photyrosine antibody (4G10, EMD Millipore) immobilized on protein G magnetic beads (protein G magnetic Sepharose, GE Healthcare). qPCR was used to quantitate encoding 55-mers in both the pre-sample (before pull-down by antibody) and post-sample (after elution with 1 mM phenyl phosphate from antibody-protein G beads).

Gene knockout studies

The dimeric CRISPR RNA-guided FokI nuclease and Csy4-based multiplex gRNA expression system was used to generate the SYK and ATG7 knockout cell lines. Two annealed target-site oligoduplexes designed by Zifit Targeter (20) and a constant region oligoduplex were assembled with BsmBI-digested pSQT1313 in a single-step ligation. 3 μ g of the ligated vector, 1 μ g of pSQT1601 expressing Csy4 RNase and RNA-guided FokI-dCas9 fusion nucleases, and 0.2 μ g of pBABE Puro were transfected into luciferase-expressing HME2 and 4T1 cells. pSQT1313 and pSQT1601 were gifts from Keith Joung (Addgene plasmids #53370 and #53369) (21). After 48 hours, cells were treated with 5 μ g/ml puromycin for clonal selection. Genomic DNA and cell lysates from selected colonies were analyzed by the PAGE-genotyping method (22) and immunoblot analyses to screen for clones with SYK or ATG7 knockout. Disruption of both alleles was confirmed by DNA sequencing.

P-body formation and clearance

Cells were treated with TGF- β 1 (R&D Systems) (10 ng/ml) for the indicated times to induce P-bodies. For P-body clearance assays, cells were washed with phosphate-buffered saline (PBS) and then allowed to recover in fresh media for the indicated times. In some experiments, the SYK inhibitor R406 (Selleckchem), or the autophagy inhibitors N2,N4-bis(phenylmethyl)-2,4-quinazolinediamine (DBEQ) (Sigma; 0.625–2.5 μ M) or chloroquine (Tocris; 10 μ M) were added during P-body clearance. For the detection of P-bodies and autophagosomes by immunofluorescence, cells were fixed with 10% ice cold methanol for 10 min, permeabilized with 1% Triton X-100 in PBS, and blocked with PBS containing 10% goat serum, 0.05% Tween 20, and 1 mg/ml BSA. Cells were immunostained using the indicated antibodies against DCP1A, p62, or phosphotyrosine. Bound primary antibodies were detected using AlexaFluor 488-conjugated goat anti-mouse IgG and/or AlexaFluor 594-conjugated goat anti-rabbit IgG secondary antibodies (Invitrogen). P-bodies were quantified using ImageJ to set a threshold mask (Otsu Thresholding Filter), which allowed only P-bodies (puncta) to be analyzed. The pixel range of P-bodies were set at a range

between 30 and 270 units. This range was considered to have staining above background. The number of P-bodies and nuclei were counted in an image or field containing at least 25 cells to determine the number of P-bodies per cell. Data are expressed as the mean \pm standard error of the mean (SEM) from 3 independent biological replicates.

In vivo metastasis

Control and ATG7-deleted 4T1 cells engineered to express firefly luciferase were resuspended in PBS (50 μ l) and orthotopically engrafted onto the second mammary fat pad of 4 week old Balb/c mice (2.5×10^4 cells/mouse) (Jackson Labs, Bar Harbor, ME). Primary tumor growth and metastasis development were assessed via weekly bioluminescent imaging using the Advanced Molecular Imager (AMI) (Spectral Instruments, Tucson, AZ). In separate experiments, 4T1 primary tumors were engrafted onto Balb/c and NRG mice and primary tumors were surgically excised when they reached 200mm³. At this point mice were split into cohorts at treated with fostamatinib (50 mg/kg; p.o./q.d.). Upon necropsy lungs from all animals were removed and fixed in 10% formalin and dehydrated in 70% ethanol for visualization of pulmonary metastatic nodules and histological analyses. All animal studies were performed in accordance with the animal protocol procedures approved by the Institutional Animal Care and Use Committee (IACUC) of Purdue University.

EMT score quantification

EMT metric previously described was applied to calculate EMT scores for various samples (23). A set of EMT-relevant predictors and cross-platform normalizer transcripts was extracted for each sample and then used to assign probabilities of belonging to E, hybrid E/M, or M phenotypes, as denoted by the ordered triple $S_i = (P_E, P_{E/M}, P_M)$. Categorization was assigned based on maximal value of this ordered triple, and then projected onto [0, 2].

Statistical analyses

2-way ANOVA or 2-sided T-tests were used where the data met the assumptions of these tests and the variance was similar between the two groups being compared. P values of less than 0.05 were considered significant. No exclusion criteria were utilized in these studies.

Results

Epithelial-mesenchymal plasticity is drives metastasis

We recently established two mesenchymal cell conditions derived from a common, HER2-transformed, human mammary epithelial cell (HME2) precursor (5). In one condition, EMT was induced upon prolonged continuous treatment (4 weeks) with the cytokine TGF- β 1 and the other was induced upon a similar length of continuous treatment with the EGFR/HER2 kinase inhibitor, lapatinib. Importantly, while both mesenchymal states are robust, only TGF- β -induced EMT was capable of undergoing MET upon withdrawal of the exogenous stimuli (5). The resultant cell populations are illustrated in Figure 1a via flow cytometric analysis of CD44 and CD24, where treatment and withdrawal of TGF- β 1 resulted in the formation of a heterogeneous population of epithelial and mesenchymal cells (Fig 1a). In contrast, lapatinib resistant cells (LAPR) derived from prolonged treatment with the kinase inhibitor remained in a mesenchymal, CD44^{hi} phenotype even after prolonged withdrawal of

the compound. We sought to evaluate the impact of these reversible versus stable EMT events on tumor growth and metastasis. Therefore, we co-engrafted the LAPR cells with the parental HME2 cells to create CD44^{hi} / CD44^{low} heterogeneous tumors, similar to the post-TGF- β 1 population. The mixture of LAPR cells with parental HME2 cells did not affect primary tumor growth and we did not observe any metastasis in mice bearing either of these tumors (Fig 1b-1d). In contrast, the post-TGF β 1 treated cells formed larger tumors and we were able to image and isolate metastases within the long bones of one of these tumor bearing mice (Fig 1b-1d). *Ex-vivo* subculture of these bone metastases (HME2-BM) led to a culture that displayed a uniform epithelial morphology similar to that of the HME2 parental cells but with diminished cell surface expression of CD24 (Fig 1d-1e). Taken together, these data indicate that EMP is critical for the metastatic progression of this HER2 transformation model.

Reversible and irreversible EMT's have similar transition intensities

We next sought to characterize unique differences in gene expression between reversible and irreversible EMT events induced by TGF- β and kinase inhibition, respectively. Following 4 weeks of treatment with TGF- β 1 or lapatinib, CD44^{hi} cells were sorted by FACS and analyzed by RNA sequencing. Both of these cell populations were compared to non-stimulated, parental HME2 cells. Numerous established markers of EMT such CDH1, Vimentin, Twist, and FGFR1 were similarly modulated by both TGF- β 1 and lapatinib treatment (Fig 2a). Only a limited set of genes were uniquely regulated between TGF- β and lapatinib-induced EMT events (Fig 2b). Pathway analysis of these gene sets did not offer obvious mechanistic explanation for these reversible versus non-reversible EMT events (Fig 2b; Supplementary Table 1). To investigate the notion that EMT becomes irreversible based on the intensity of an EMT, we utilized our recently developed inferential model of quantifying the extent of EMT in a given sample (23). This metric uses canonical epithelial and mesenchymal markers to compute the 'EMT score' on a scale of 0 (fully epithelial) to 2 (fully mesenchymal). These analyses indicated that both TGF- β 1 and lapatinib induced similar EMT intensities (Fig 2c). These analyses suggest that the reversible nature of EMT is determined via the nature of the inducing stimuli as opposed to the intensity of the transition.

SYK activity is increased upon TGF- β -induced EMT

To further characterize post-transcriptional differences that may be regulating EMP, we conducted an analysis of kinase activity using a peptide-substrate microarray on the PamStation-12 platform. This platform is capable of quantifying the differential phosphorylation of 142 serine/threonine containing peptides and 140 different tyrosine containing peptides upon incubation with cell lysates. This analysis detected an moderate decrease in phosphorylation of a peptide containing the autophosphorylation sites found within the activation loop of SYK, containing tyrosine 525 and 526 (Supplementary Table 2; (24)). However, consistent with previous studies, we observed SYK mRNA expression to be drastically downregulated upon treatment with TGF- β (6). Moreover, use of the KM plotter analysis tool indicated that diminished SYK mRNA expression is strongly associated with decreased breast cancer patient survival (Fig 3a; (25)). Therefore, we normalized the peptide phosphorylation values to SYK mRNA expression reads from our RNA sequence analyses.

Use of this approach clearly demonstrated that, while SYK expression was downregulated by TGF- β -induced EMT, the activity of the remaining pool was dramatically increased (Fig 3b). Consistent with our RNA sequence analyses, immunoblotting of whole cell lysates demonstrated a robust decrease in the total levels of SYK in TGF- β -treated and Lapatinib-resistant cells (Fig 3c). Differential phosphorylation of Y525/526 of endogenous SYK was not detectable in any of these samples, potentially due to the dramatic reduction in total SYK during EMT (Fig 3c, Supplementary Fig 1). Therefore, to verify enhanced SYK activity following TGF- β -induced EMT, we conducted a substrate phosphorylation assay using SYK PhageTIDE, a peptide sequence (EDPDYEQPSA) identified by phage display to be a highly specific and sensitive substrate for SYK as compared to the Y525/526 containing activation loop autophosphorylation peptide (19,26). This peptide was conjugated to a DNA oligonucleotide, allowing for highly sensitive quantification of phosphorylated peptide via PCR following its capture using the antityrosine antibody 4G10. Using this ultrasensitive approach, we were able to clearly demonstrate enhanced SYK activity specifically in HME2 cells induced to undergo EMT by TGF- β as compared to Lapatinib-induced EMT (Fig 3d). Taken together these data clearly indicate that in contrast to diminished total expression levels of SYK, its kinase activity was upregulated in a reversible, but not an irreversible EMT.

SYK is present in P-bodies and facilitates their clearance during MET

We have recently demonstrated that induction of EMT by TGF- β induces the formation of cytoplasmic RNA processing complexes called P-bodies, and clearance of P-bodies through autophagy is required for reversal of EMT (15). Based on our previous identification of a role for SYK in promoting stress granule clearance through autophagy and our identification of multiple P-body proteins as SYK substrates, we next sought to assess a role for SYK in P-body formation and clearance (27)(11). Expression of mCherry labeled SYK results in a cellular diffuse localization (Fig 4a). However, coexpression of the P-body structural protein, DCP1A leads to formation of large P-bodies and SYK clearly concentrated into these structures (Fig 4a). This dramatic change in SYK localization occurred in 100% of cells containing P-bodies (Supplementary figure 2). Despite the relative insolubility of P-body complexes, we were able to use immunoprecipitation to demonstrate association of EGFP-DCP1A with a GST tagged SYK (Fig 4b). Consistent with SYK activity within P-bodies, we observed a dramatic increase in phosphotyrosine staining in P-bodies selectively within cells overexpressing SYK (Fig 4c). Normal murine mammary gland (NMuMG) cells are highly responsive to TGF- β -induced EMT, and form robust P-bodies during this process (15). Therefore, we treated control and SYK overexpressing NMuMG cells with TGF- β 1 for 48 hours to induce P-body formation. At this point the TGF- β was removed and cells were placed in fresh media for an additional 24 hours to allow for P-body clearance. The induction of P-bodies was not affected by SYK overexpression, but the clearance of P-bodies after TGF- β removal was significantly increased (Fig. 4d and 4e). This SYK-mediated clearance of the P-bodies was prevented by inhibition of autophagy through blockade of endosomal acidification using the antimalarial drug, chloroquine, during the recovery period following TGF- β -induced EMT (Fig 4f). Taken together, these data are consistent with a model in which SYK physically concentrates into P-bodies upon TGF- β -induced EMT and functions to promote their autophagic clearance during MET.

SYK activity is required for mesenchymal-epithelial transition

To determine the necessity of SYK in the ability of cells to undergo EMT and MET we deleted *SYK* from the HME2 cells using a genome editing approach (Fig 5a; (15)). Complete absence of SYK led to an accumulation of P-bodies and prevented P-body clearance following TGF- β -induced EMT (Fig 5b-c). To focus on the role of SYK kinase activity in P-body clearance and execution of the MET process we treated cells with TGF- β and allowed them to recover in the absence or presence of the SYK inhibitor R406. Association of p62/Sequestosome-1 with LC3 targets these proteins to autophagosomes where they are degraded selectively through autophagy. Similar to DCP1A, when autophagy is inhibited p62-positive inclusion bodies accumulate (28,29). Consistent with a role of SYK activity in autophagy-mediated clearance of P-bodies, we observed robust accumulation of p62 and DCP1A containing vesicles when R406 was included during recovery from TGF- β treatment (Fig 5d). Following a 4-week treatment of the HME2 cells with TGF- β 1 a 2-week recovery period allowed levels of Epithelial-cadherin (Ecad) to return (Fig 5e). When R406 was added during the recovery phase, however, return of Ecad was attenuated (Fig 5e). Consistent with our previous report (14), addition of the autophagy inhibitor DBeQ similarly prevented cells from undergoing MET subsequent to TGF- β 1 treatment and withdrawal (Supplementary figure 3). The onset of TGF- β 1-induced EMT can easily be visualized via bright field microscopy with all cells displaying a mesenchymal morphology (Fig. 5f). This was also quantified by a CD44^{hi} flow cytometric phenotype (Fig 5g). This approach clearly indicated that R406 prevents the ability of cells to undergo MET following TGF- β 1-induced EMT (Fig 5e-5g). These results suggest that SYK activity facilitates autophagy-mediated P-body clearance during MET.

Inhibition of autophagy stabilizes a mesenchymal phenotype and inhibits metastasis

Using an *in vivo* reporter system, we have previously established that highly metastatic 4T1 cells are very dynamic and undergo EMT and MET during initiation of growth in 3D culture and during *in vivo* tumor formation and metastasis (30,31). To establish the necessity of autophagy-mediated MET for metastasis, we again utilized a genomic editing approach to delete the autophagy mediator, ATG7 (Fig 6a). Consistent with the dynamic EMP phenotype of the 4T1 cells and the requirement of autophagy for MET, deletion of ATG7 led to stabilization of a mesenchymal phenotype that included the accumulation of P-bodies (Fig 6a and 6b; Supplementary fig 4). Correspondingly, deletion of ATG7 prevented efficient growth within a compliant 3D culture environment (Fig 6c). Deletion of ATG7 had a minimal effect on primary tumor growth within the mammary fat pad (Fig 6d). Histologically, ATG7 deleted tumors displayed a similar mesenchymal morphology, characteristic of 4T1 primary tumors, and cell proliferation was not affected (Fig 6e). In contrast, deletion of ATG7 led to a complete inhibition of pulmonary metastasis as measured by longitudinal bioluminescence and endpoint enumeration of metastatic nodules (Fig 6f-6h). Taken together these data strongly suggest that highly metastatic cells consistently transition between epithelial and mesenchymal phenotypes, and autophagy is required for the efficient execution of MET and metastatic progression.

Pharmacological inhibition of SYK stabilizes a mesenchymal morphology and inhibits metastatic outgrowth

Consistent with our ATG7 genetic data, previous studies indicate that inhibition of autophagy, through the use of chloroquine, effectively inhibits the pulmonary metastasis of 4T1 tumors (32). In attempts to improve the pharmacological specificity of targeting autophagy as an anti-metastatic therapy, we sought to evaluate the impact of SYK inhibition in the 4T1 model. *In vitro*, treatment of 4T1 cells with R406 stabilized a mesenchymal morphology, and potently inhibited tumor cell growth in 3D culture conditions (Fig 7a and 7b). We next conducted *in vivo* studies using the clinically approved pro-drug of R406, fostamatinib (33). To specifically focus on inhibition of metastasis, we established primary mammary fat pad tumors for a period of 2 weeks, and only after surgical resection of these primary tumors were mice treated with fostamatinib (Fig 7c). This approach confirmed that systemic inhibition of SYK is capable of inhibiting the pulmonary metastatic outgrowth of 4T1 cells (Fig 7d and 7f). Consistent with a role of SYK in MET, micrometastases that were located in the fostamatinib-treated group failed to regain Ecad expression as compared to similar sized lesions in untreated animals (Fig 7g).

Discussion

Transient suppression of a differentiated epithelial phenotype by breast cancer cells is strongly associated with an increased invasive phenotype and perpetuation of the early steps of metastasis (34). Mesenchymal cells also have an increased capacity to persist in the presence of chemotherapy (4,35,36). Our previous studies and our data herein are consistent with the notion that autophagy drives the MET process and efficient progression to macroscopic tumor formation (15). Our findings are strongly supported by recent studies indicating autophagy facilitates a dormant-to-proliferative switch by tumors cells within the lungs (16). Therefore, autophagy is intimately linked to the plasticity of tumor cells to transition between epithelial and mesenchymal states, processes that are critical for dissemination, drug resistance and metastatic outgrowth.

In addition to chemotherapy numerous studies indicate that when cells transition into a mesenchymal state they also become highly resistant to kinase inhibitors, antibody therapies, and even immunotherapy (37)(38)(39). Therefore, the goal of complete eradication of these dormant, highly drug resistant subpopulations may be unattainable. Herein, we explored approaches to pharmacologically maintain populations of disseminated cells in an asymptomatic state by preventing their reversion back to an epithelial state. By combined genetic and kinase activity analyses, we were able to identify SYK as being strongly activated in mesenchymal cells that are capable of reverting back to an epithelial phenotype and giving rise to lung and long bone metastases. The role of SYK in this process is to promote the removal of P-bodies through autophagy, an event that supports MET following initiation of metastatic outgrowth.

Our findings also emphasize the importance of properly interpreting data within publicly available databases that are largely based on mRNA and protein expression values (40,41) (42). There are examples, such as HER2, where enhanced expression of kinases drives their auto activation and predicts for sensitivity to inhibitors. The corollary, however, is not well

established. Indeed, mRNA expression analyses demonstrate a strong correlation between decreased SYK expression and improved patient survival, suggesting it functions as a tumor suppressor (8). However, our data clearly indicate that although SYK expression is dramatically inhibited with TGF- β , its activity is increased on a per-molecule level and it is spatially concentrated into P-bodies. The mechanisms of SYK activation and translocation to P-bodies, following TGF- β -induced EMT are yet to be established and are currently under investigation in our laboratory. However, the presence of high levels of phosphotyrosine in P-bodies and stress granules (27), suggests that SYK associates with ribonucleoprotein particles when it is in an activated state.

We also suggest the diagnostic utility of substrate kinase assays to overcome the pitfalls of gene expression analyses. Our oligonucleotide-peptide conjugate approach offers an extremely sensitive method to quantify kinase activity. The approach herein utilized a single peptide substrate optimized for SYK specificity (19). However, our qPCR-based readout presents the opportunity to utilize oligonucleotides with unique bar codes flanked by shared priming sequences linked to a variety of substrate-specific peptides, which is the subject of a forthcoming manuscript. This approach will allow for quantitative readouts of multiple kinase substrates all within a single reaction (11). Clearly, this type of enzymatic activity-based diagnostic that can be conducted in a single reaction on small amounts of tissue holds great promise for predicting personalized cancer therapeutics.

SYK is well established as a key signaling molecule in B-cell activation. As such, fostamatinib was developed and has shown clinical efficacy for the treatment of B-cell associated diseases such as rheumatoid arthritis and lymphoma (24,43). Furthermore, fostamatinib was recently approved for the treatment of chronic immune thrombocytopenia (ITP). Our data suggest repurposing of fostamatinib as an effective treatment for the prevention of metastatic recurrence in breast cancer. The clinical trial parameters for this type of recurrence prevention strategy are difficult. However, fostamatinib might be particularly suited for this approach given it was developed as a long-term therapeutic for treatment of a chronic disease and thus has a very low toxicity profile (44,45). In addition to the tumor cell autonomous effects presented herein, systemic treatment with fostamatinib also prevents B-cell-mediated promotion of a protumorigenic microenvironment (46,47). Understanding this potential polypharmacology upon systemic treatment with fostamatinib clearly warrants further investigation.

Overall, the current studies have utilized a variety of genetic, proteomic and pharmacological techniques to demonstrate that SYK activity and ATG7-mediated autophagy are required for MET, the vital final step in formation of macroscopic metastases. More broadly, our work also highlights an exit from the traditional pharmacological goal of total tumor cell eradication and instead posits the concept of forced tumor dormancy for the management of stage IV breast cancer.

Supplementary Material

Refer to Web version on PubMed Central for supplementary material.

Acknowledgments

This research was supported in part by the American Cancer Society (RSG-CSM130259) to MKW and the National Institutes of Health (R01CA207751 to MKW and R01AI098132 to RLG) and Purdue Center for Cancer Research via an NIH NCI grant (P30CA023168). MKJ is also supported by a training fellowship from the Gulf Coast Consortia on the Computational Cancer Biology Training Program (Cancer Prevention and Research Institute of Texas (CPRIT) grant no. RP170593). We acknowledge Carol Post for her insightful comments. We acknowledge Yixing Sun for preparation of the SYKtide-DNA conjugate. We kindly acknowledge the expertise of the personnel within the Purdue Center for Cancer Research Biological Evaluation Core. We also acknowledge the use of the facilities within the Bindley Bioscience Center, a core facility of the NIH-funded Indiana Clinical and Translational Sciences Institute.

References

1. Steeg PS. Targeting metastasis. *Nat Rev Cancer*. 2016;16:201–18. [PubMed: 27009393]
2. Wendt MK, Tian M, Schiemann WP. Deconstructing the mechanisms and consequences of TGF- β -induced EMT during cancer progression. *Cell Tissue Res* 2012;347:85–101. [PubMed: 21691718]
3. Mani SA, Guo W, Liao M-J, Eaton EN, Ayyanan A, Zhou AY, et al. The epithelial-mesenchymal transition generates cells with properties of stem cells. *Cell*. 2008;133:704–15. [PubMed: 18485877]
4. Luo M, Brooks M, Wicha MS. Epithelial-mesenchymal plasticity of breast cancer stem cells: implications for metastasis and therapeutic resistance. *Curr Pharm Des* 2015;21:1301–10. [PubMed: 25506895]
5. Brown WS, Akhand SS, Wendt MK, Brown WS, Salehin Akhand S, Wendt MK. FGFR signaling maintains a drug persistent cell population following epithelial-mesenchymal transition. *Oncotarget* 2016;7:83424–36. [PubMed: 27825137]
6. Taube JH, Herschkowitz JI, Komurov K, Zhou AY, Gupta S, Yang J, et al. Core epithelial-to-mesenchymal transition interactome gene-expression signature is associated with claudin-low and metaplastic breast cancer subtypes. *Proc Natl Acad Sci U S A*. 2010;107:15449–54. [PubMed: 20713713]
7. Singh A, Greninger P, Rhodes D, Koopman L, Violette S, Bardeesy N, et al. A gene expression signature associated with “K-Ras addiction” reveals regulators of EMT and tumor cell survival. *Cancer Cell*. 2009;15:489–500. [PubMed: 19477428]
8. Sung YM, Xu X, Sun J, Mueller D, Sentissi K, Johnson P, et al. Tumor Suppressor Function of Syk in Human MCF10A In Vitro and Normal Mouse Mammary Epithelium In Vivo. *PLOS ONE*. 2009;4:e7445. [PubMed: 19829710]
9. Yuan Y, Liu H, Sahin A, Dai JL. Reactivation of SYK expression by inhibition of DNA methylation suppresses breast cancer cell invasiveness. *Int J Cancer*. 2005;113:654–9. [PubMed: 15455373]
10. Jetson RR, Krusemark CJ. Sensing Enzymatic Activity by Exposure and Selection of DNA-Encoded Probes. *Angew Chem Int Ed* 2016;55:9562–6.
11. Kim D, Jetson RR, Krusemark CJ. A DNA-assisted immunoassay for enzyme activity via a DNA-linked, activity-based probe. *Chem Commun Camb Engl* 2017;53:9474–7.
12. Iliuk AB, Martin VA, Alicie BM, Geahlen RL, Tao WA. In-depth analyses of kinase-dependent tyrosine phosphoproteomes based on metal ion-functionalized soluble nanopolymers. *Mol Cell Proteomics MCP*. 2010;9:2162–72. [PubMed: 20562096]
13. Parker R, Sheth U. P bodies and the control of mRNA translation and degradation. *Mol Cell* 2007;25:635–46. [PubMed: 17349952]
14. Zheng D, Chen C-YA, Shyu A-B. Unraveling regulation and new components of human P-bodies through a protein interaction framework and experimental validation. *RNA N Y N*. 2011;17:1619–34.
15. Hardy SD, Shinde A, Wang W-H, Wendt MK, Geahlen RL. Regulation of epithelial-mesenchymal transition and metastasis by TGF- β , P-bodies, and autophagy. *Oncotarget* 2017;8:103302–14. [PubMed: 29262563]

16. Vera-Ramirez L, Vodnala SK, Nini R, Hunter KW, Green JE. Autophagy promotes the survival of dormant breast cancer cells and metastatic tumour recurrence. *Nat Commun* 2018;9:1944. [PubMed: 29789598]
17. Mowers EE, Sharifi MN, Macleod KF. Autophagy in cancer metastasis. *Oncogene* 2017;36:1619–30. [PubMed: 27593926]
18. Brown WS, Tan L, Smith A, Gray NS, Wendt MK. Covalent Targeting of Fibroblast Growth Factor Receptor Inhibits Metastatic Breast Cancer. *Mol Cancer Ther* 2016;15:2096–106. [PubMed: 27371729]
19. Schmitz R, Baumann G, Gram H. Catalytic specificity of phosphotyrosine kinases Blk, Lyn, c-Src and Syk as assessed by phage display. *J Mol Biol* 1996;260:664–77. [PubMed: 8709147]
20. Sander JD, Maeder ML, Reyon D, Voytas DF, Joung JK, Dobbs D. ZiFiT (Zinc Finger Targeter): an updated zinc finger engineering tool. *Nucleic Acids Res* 2010;38:W462–468. [PubMed: 20435679]
21. Wyvekens N, Topkar VV, Khayter C, Joung JK, Tsai SQ. Dimeric CRISPR RNA-Guided FokI-dCas9 Nucleases Directed by Truncated gRNAs for Highly Specific Genome Editing. *Hum Gene Ther* 2015;26:425–31. [PubMed: 26068112]
22. Zhu X, Xu Y, Yu S, Lu L, Ding M, Cheng J, et al. An efficient genotyping method for genome-modified animals and human cells generated with CRISPR/Cas9 system. *Sci Rep* 2014;4:6420. [PubMed: 25236476]
23. George JT, Jolly MK, Xu J, Somarelli J, Levine H. Survival outcomes in cancer patients predicted by a partial EMT gene expression scoring metric. *Cancer Res* 2017;canres.3521.2016.
24. Hoellenriegel J, Coffey GP, Sinha U, Pandey A, Sivina M, Ferrajoli A, et al. Selective, novel spleen tyrosine kinase (Syk) inhibitors suppress chronic lymphocytic leukemia B-cell activation and migration. *Leukemia*. 2012;26:1576–83. [PubMed: 22362000]
25. Lánckzy A, Nagy Á, Bottai G, Munkácsy G, Szabó A, Santarpia L, et al. miRpower: a web-tool to validate survival-associated miRNAs utilizing expression data from 2178 breast cancer patients. *Breast Cancer Res Treat*. 2016;160:439–46. [PubMed: 27744485]
26. Lipchik AM, Killins RL, Geahlen RL, Parker LL. A peptide-based biosensor assay to detect intracellular Syk kinase activation and inhibition. *Biochemistry*. 2012;51:7515–24. [PubMed: 22920457]
27. Krisenko MO, Higgins RL, Ghosh S, Zhou Q, Trybula JS, Wang W-H, et al. Syk Is Recruited to Stress Granules and Promotes Their Clearance through Autophagy. *J Biol Chem*. 2015;290:27803–15. [PubMed: 26429917]
28. Komatsu M, Ichimura Y. Physiological significance of selective degradation of p62 by autophagy. *FEBS Lett* 2010;584:1374–8. [PubMed: 20153326]
29. Ichimura Y, Komatsu M. Selective degradation of p62 by autophagy. *Semin Immunopathol* 2010;32:431–6. [PubMed: 20814791]
30. Wendt MK, Taylor MA, Schiemann BJ, Sossey-Alaoui K, Schiemann WP. Fibroblast growth factor receptor splice variants are stable markers of oncogenic transforming growth factor β 1 signaling in metastatic breast cancers. *Breast Cancer Res BCR*. 2014;16:R24. [PubMed: 24618085]
31. Wendt MK, Taylor MA, Schiemann BJ, Schiemann WP. Down-regulation of epithelial cadherin is required to initiate metastatic outgrowth of breast cancer. *Mol Biol Cell* 2011;22:2423–35. [PubMed: 21613543]
32. Antitumor and antimetastatic activities of chloroquine diphosphate in a murine model of breast cancer - ScienceDirect [Internet]. [cited 2018 4 30]. Available from: <https://www.sciencedirect.com/science/article/pii/S0753332210001174?via%3Dihub#fig0025>
33. Braselmann S, Taylor V, Zhao H, Wang S, Sylvain C, Baluom M, et al. R406, an Orally Available Spleen Tyrosine Kinase Inhibitor Blocks Fc Receptor Signaling and Reduces Immune Complex-Mediated Inflammation. *J Pharmacol Exp Ther* 2006;319:998–1008. [PubMed: 16946104]
34. Pastushenko I, Brisebarre A, Sifrim A, Fioramonti M, Revenco T, Boumahdi S, et al. Identification of the tumour transition states occurring during EMT. *Nature*. 2018;1.
35. Schmidt JM, Panzilius E, Bartsch HS, Irmeler M, Beckers J, Kari V, et al. Stem-Cell-like Properties and Epithelial Plasticity Arise as Stable Traits after Transient Twist1 Activation. *Cell Rep* 2015;10:131–9. [PubMed: 25578726]

36. Singh A, Settleman J. EMT, cancer stem cells and drug resistance: an emerging axis of evil in the war on cancer. *Oncogene*. 2010;29:4741–51. [PubMed: 20531305]
37. Akalay I, Janji B, Hasmim M, Noman MZ, André F, De Cremoux P, et al. Epithelial-to-mesenchymal transition and autophagy induction in breast carcinoma promote escape from T-cell-mediated lysis. *Cancer Res* 2013;73:2418–27. [PubMed: 23436798]
38. Dongre A, Rashidian M, Reinhardt F, Bagnato A, Keckesova Z, Ploegh HL, et al. Epithelial-to-Mesenchymal Transition Contributes to Immunosuppression in Breast Carcinomas. *Cancer Res* 2017;77:3982–9. [PubMed: 28428275]
39. Burnett JP, Korkaya H, Ouzounova MD, Jiang H, Conley SJ, Newman BW, et al. Trastuzumab resistance induces EMT to transform HER2(+) PTEN(–) to a triple negative breast cancer that requires unique treatment options. *Sci Rep* 2015;5:15821. [PubMed: 26522776]
40. Curtis C, Shah SP, Chin S-F, Turashvili G, Rueda OM, Dunning MJ, et al. The genomic and transcriptomic architecture of 2,000 breast tumours reveals novel subgroups. *Nature*. 2012;486:346–52. [PubMed: 22522925]
41. Ciriello G, Gatza ML, Beck AH, Wilkerson MD, Rhie SK, Pastore A, et al. Comprehensive Molecular Portraits of Invasive Lobular Breast Cancer. *Cell*. 2015;163:506–19. [PubMed: 26451490]
42. Gy rffy B, Surowiak P, Budczies J, Lánczky A. Online survival analysis software to assess the prognostic value of biomarkers using transcriptomic data in non-small-cell lung cancer. *PloS One*. 2013;8:e82241. [PubMed: 24367507]
43. Friedberg JW, Sharman J, Sweetenham J, Johnston PB, Vose JM, LaCasce A, et al. Inhibition of Syk with fostamatinib disodium has significant clinical activity in non-Hodgkin lymphoma and chronic lymphocytic leukemia. *Blood*. 2010;115:2578–85. [PubMed: 19965662]
44. Bussel JB, Arnold DM, Cooper N, Khalafallah AA, Boxer M, Liles D, et al. Long-Term Maintenance of Platelet Responses in Adult Patients with Persistent/Chronic Immune Thrombocytopenia Treated with Fostamatinib: 1-Year Efficacy and Safety Results. *Blood*. 2017;130:16–16.
45. McKeage K, Lyseng-Williamson KA. Fostamatinib in chronic immune thrombocytopenia: a profile of its use in the USA. *Drugs Ther Perspect*. 2018;34:451–6. [PubMed: 30459507]
46. B Cells Regulate Macrophage Phenotype and Response to Chemotherapy in Squamous Carcinomas - ScienceDirect [Internet]. [cited 2018 4 19]. Available from: <https://www.sciencedirect.com/science/article/pii/S1535610814001883>
47. Gunderson AJ, Coussens LM. B cells and their Mediators as Targets for Therapy in Solid Tumors. *Exp Cell Res* 2013;319:1644–9. [PubMed: 23499742]

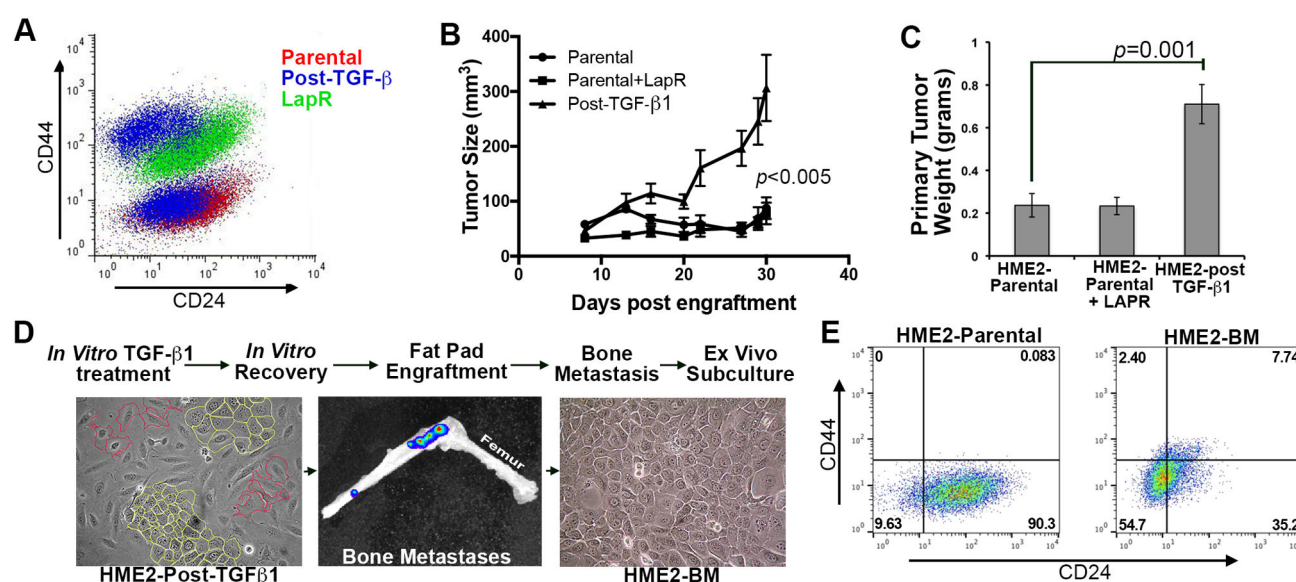


Figure 1. Epithelial-mesenchymal plasticity is required for metastasis.

(A) HER2 transformed HMLE cells (HME2) were treated with TGF- β 1 (5 ng/ml every three days) or the HER2/EGFR kinase inhibitor lapatinib (1 μ M every three days) for 4 weeks. Following an additional 4 weeks of culture in the absence of these stimuli the post-TGF- β and lapatinib resistant (LAPR) cells were analyzed by flow cytometry for expression of CD44 and CD24. Untreated (Parental) cells served as a control. (B and C) The cell populations shown in panel A were engrafted onto the mammary fat pad of NSG mice and primary tumor size was measured by digital calipers at the indicated time points. Primary tumor weights were measured 30 days after engraftment following surgical resection. Data in B and C are the mean \pm SD of three mice per group, resulting in the indicated P values. (D) Forty-five days after removal of the primary tumor, long bone metastases were detected in a post-TGF- β tumor bearing mouse. These metastases were subcultured to yield the HME2-bone metastatic (HME2-BM) cell line. (E) The HME2-BM cells were characterized via flow cytometric analysis of CD44 and CD24.

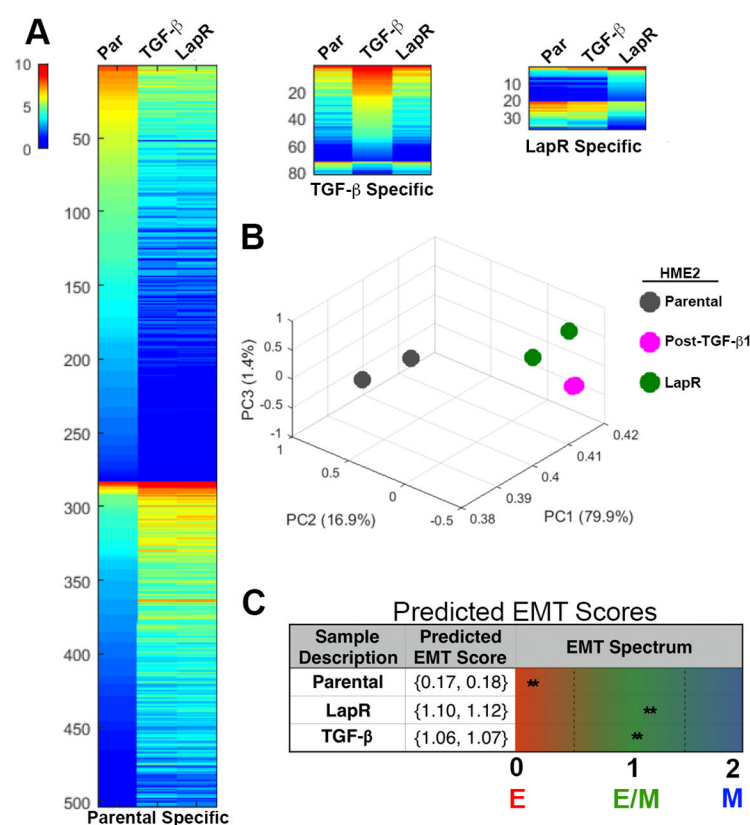


Figure 2. Reversible and irreversible EMT's have similar transition intensities.

(A) Heat map representation of the differentially expressed genes determined by RNA-sequence analyses of parental HME2 cells (Par) as compared to HME2 cells treated with TGF- β 1 (5ng/ml every 3 days for 4 weeks) and those selected for resistance to lapatinib (LAPR; 1 μ M every 3 days for 4 weeks). (B) Principle component analyses of the duplicate gene expression analyses described in panel A. (C) EMT score analysis of differential gene expression for the indicated cell populations.

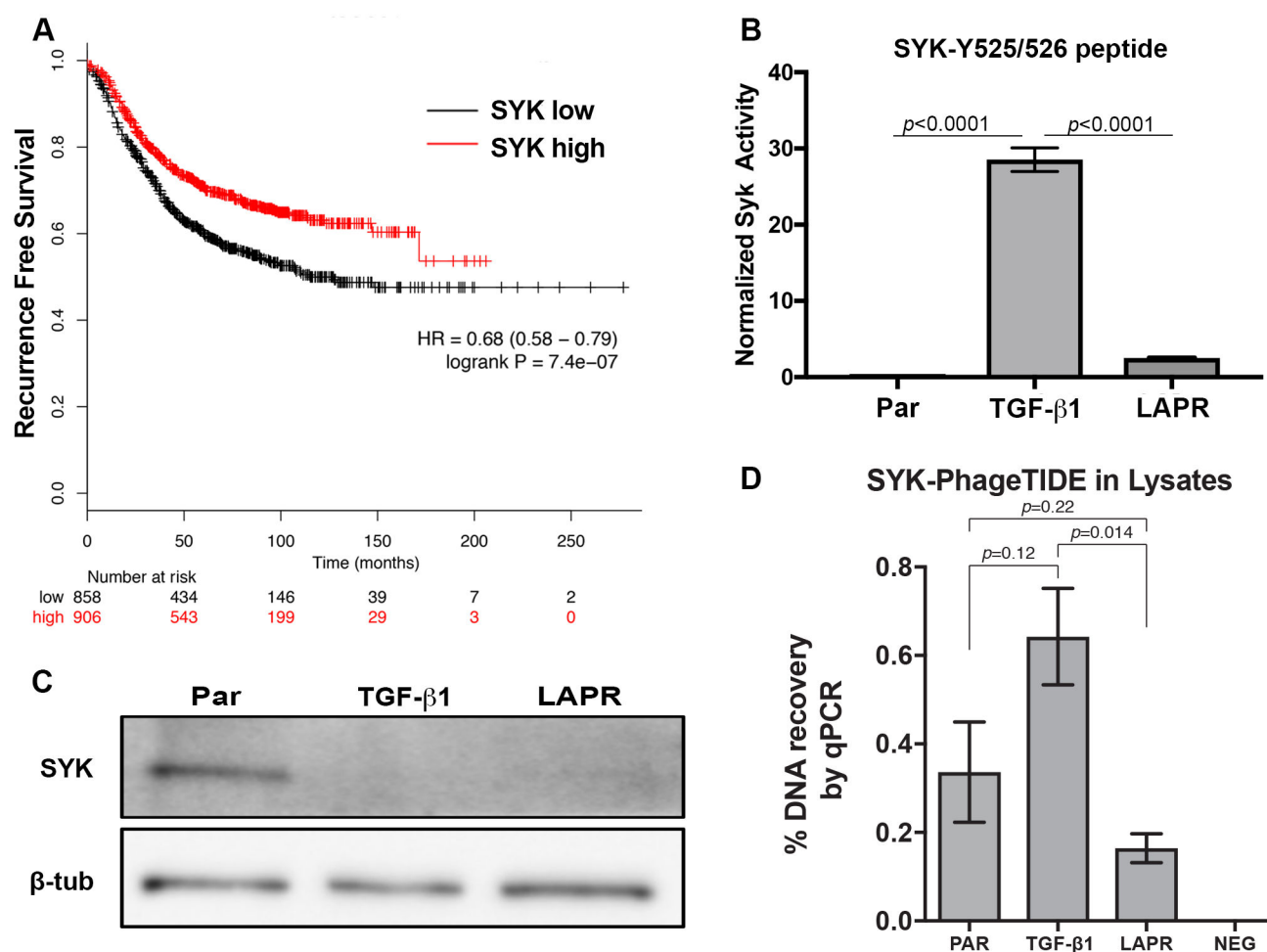


Figure 3. Spleen tyrosine kinase activity is specifically increased following TGF- β -induced EMT. (A) Kaplan Meier analysis of recurrence free survival based on the median expression value of SYK. Data were obtained from the indicated patient numbers, using the KM plotter online analysis tool, resulting the indicated P value. (B) Substrate phosphorylation intensity determined for a peptide containing the SYK autophosphorylation (Y525/Y526) site in HME2 parental, lapatinib resistant (LAPR) and TGF- β treated cells. Data are normalized to SYK mRNA expression values determined by RNA sequence analysis for these same samples. Data are mean \pm SD of three substrate phosphorylation analyses resulting in the indicated P value. (C) Immunoblot analysis of total SYK in HME2 parental, lapatinib resistant (LAPR) and TGF- β treated cells. β -tubulin was assessed as a loading control. (D) Quantification of SYK activity in the indicated cell populations using a DNA-conjugated SYK specific substrate peptide (SYK-PhageTIDE). Data are mean \pm SD of the signal for three unique 55-mer encoding constructs in a lysate sample resulting in the indicated P values.

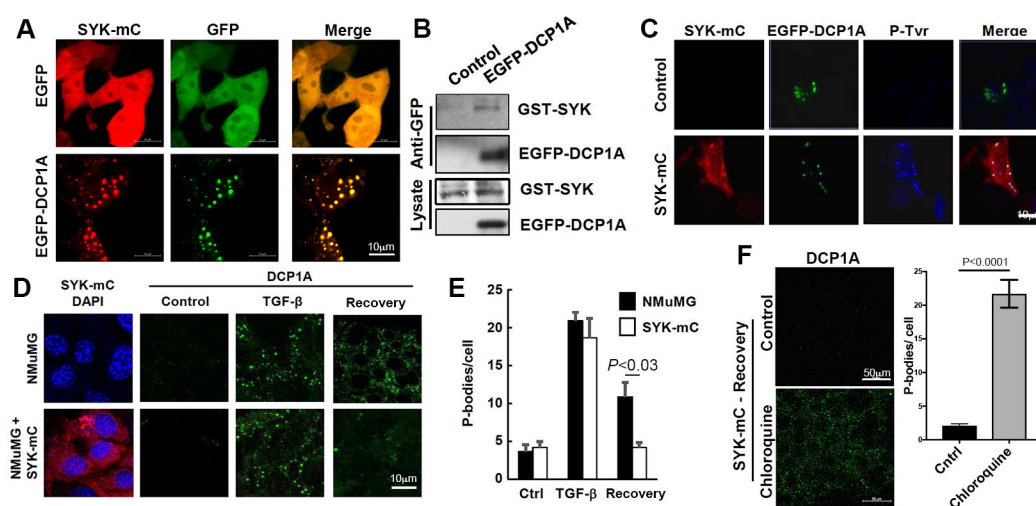
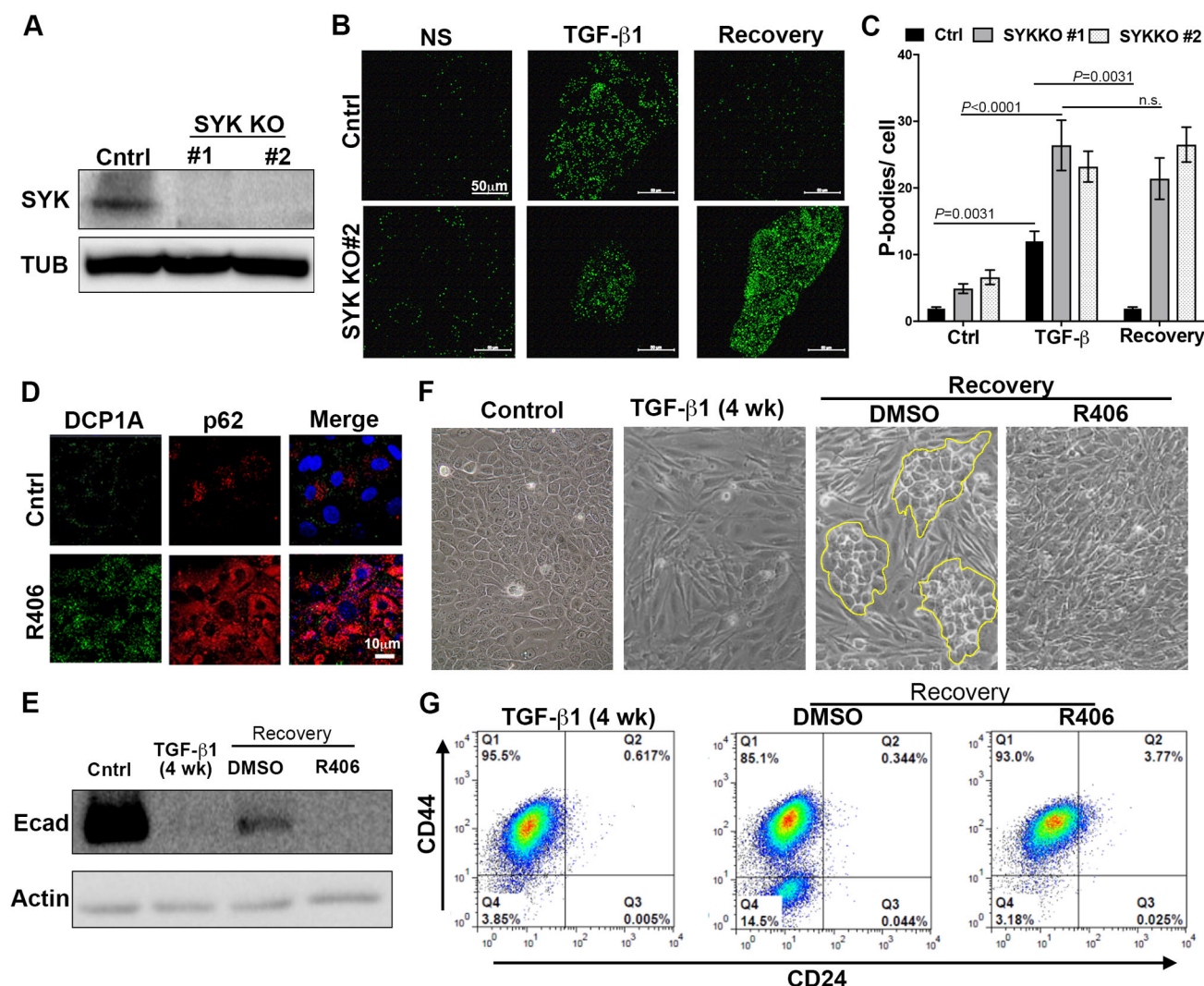


Figure 4. SYK enhances the clearance of TGF- β -induced P-bodies.

(A) HEK293 cells were transiently transfected with SYK-mCherry (SYK-mC) and EGFP as a control or EGFP-DCP1A to induce P-body formation. Localization of SYK into P-bodies was examined by fluorescence microscopy. (B) HEK293 cells expressing GST-SYK were transiently transfected to express EGFP-DCP1A, which was immunoprecipitated from cell lysates using GFP-Trap agarose beads. Proteins in immune complexes (Anti-GFP) and the cell lysate were detected using antibodies against GST (GST-SYK) and EGFP (EGFP-DCP1A). (C) Control and SYK-mCherry (SYK-mC) expressing HEK293 cells were transiently transfected with EGFP-DCP1A to induce P-bodies. After transfection, the cells were stained using antibodies against phosphotyrosine (P-Tyr) and cells were examined by fluorescence confocal microscopy to visualize colocalization of SYK, DCP1A and P-Tyr. (D) Control NMuMG cells and those stably expressing SYK-mC were left untreated (Control) or treated with TGF- β 1 for 48 hours. Where indicated, cells were allowed to recover in the absence of TGF- β (Recovery) for an additional 24 hours. Cells were fixed and stained for DCP1A (green). (E) Quantification of the average number of P-bodies per cell \pm SEM ($n > 150$ cells per treatment) for triplicate experiments resulting in the indicated P value. (F) NMuMG cells stably expressing SYK-mC were treated with TGF- β 1 and allowed to recover as in panel D. Where indicated the autophagy inhibitor chloroquine was added during the recovery period and cells were fixed and stained for DCP1A (green). P-bodies were quantified as above resulting in the indicated P value.



described in panel E. The epithelial and mesenchymal morphologies under these conditions were visualized by phase contrast microscopy. The yellow outline denotes the return of morphologically epithelial cells following treatment and recovery from TGF- β 1. (G) HME2 cells were treated as in panel B and analyzed by flow cytometry for cell surface expression of CD24 and CD44.

Author Manuscript

Author Manuscript

Author Manuscript

Author Manuscript

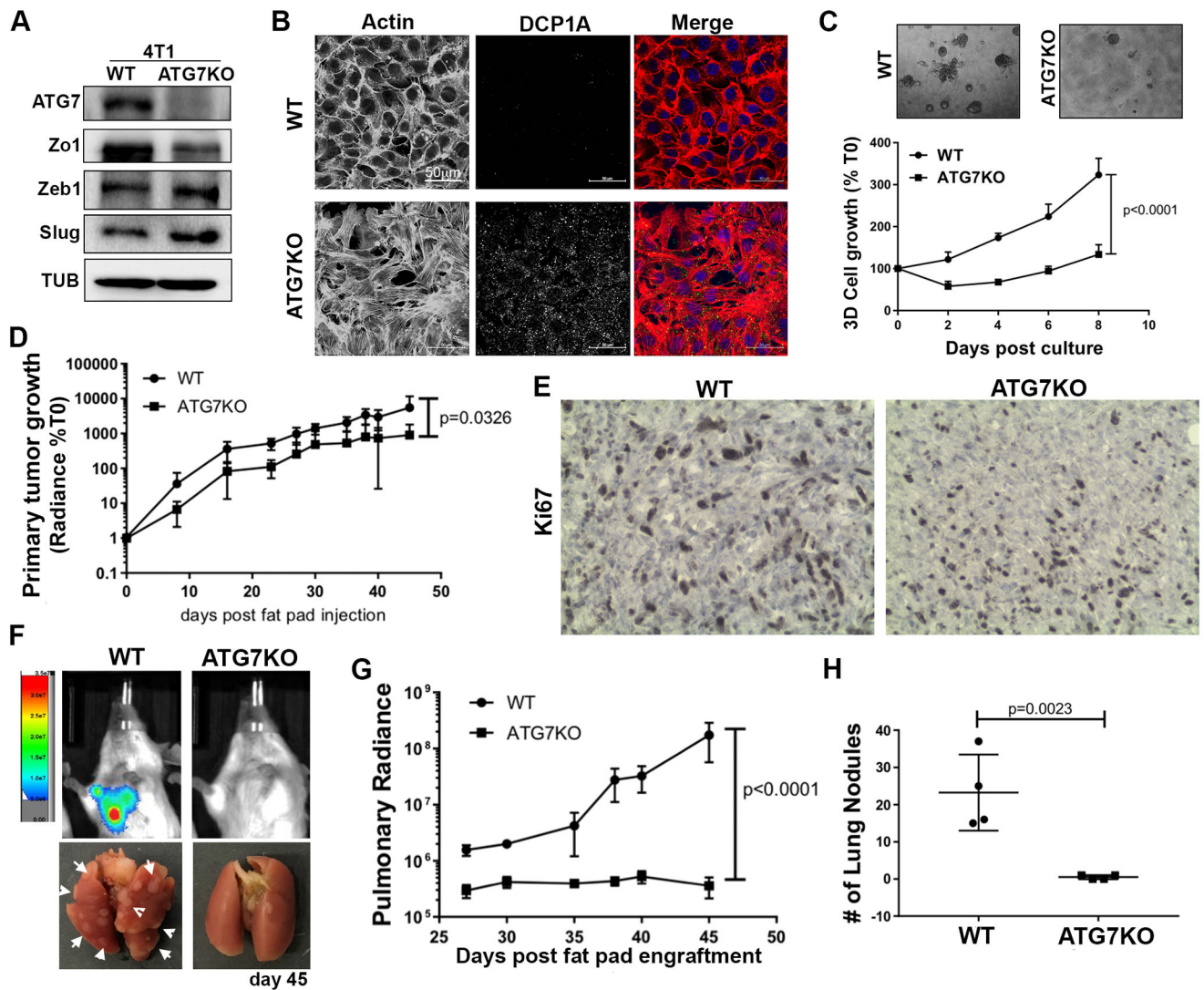


Figure 6. Autophagy is required for MET and metastasis.

(A) Genetic knockout of ATG7 (ATG7KO) in the 4T1 cells was verified by immunoblot. These same cell lysates were also analyzed for the EMT markers, Zo1, Zeb1 and Slug. Expression of Actin served as a loading control. (B) Control (WT) and ATG7KO 4T1 cells were stained with phalloidin to visualize differential organization of the actin cytoskeleton and DCP1A to visualize P-bodies. These cells were counterstained with DAPI to visualize the nucleus. (C) Control (WT) and ATG7KO 4T1 cells were grown under single cell 3D culture conditions. Longitudinal cellular outgrowth was quantified by bioluminescence at the indicated time points. Data are normalized to the plated values and are the mean \pm SD of three independent analyses resulting in the indicated P-value. (D) Control (WT) and ATG7KO 4T1 cells were engrafted onto the mammary fat pad and primary tumor growth was quantified by bioluminescence at the indicated time points. Data are normalized the injected values. (E) Immunohistochemistry for Ki67 expression in control (WT) and ATG7KO primary tumors. (F) Bioluminescent images and the corresponding gross anatomical views of lungs from control 4T1 (WT) tumor bearing mice and those bearing

ATG7KO tumors. Arrows indicate metastatic nodules. (G) Quantification of bioluminescent radiance from the pulmonary region of WT and ATG7KO tumor bearing mice at the indicated time points. (H) Upon necropsy the numbers of pulmonary metastatic nodules were quantified for both control (WT) and ATG7KO 4T1 tumor bearing mice. For panels D, G, and H, data are the mean \pm SE of 5 mice resulting in the indicated P values.

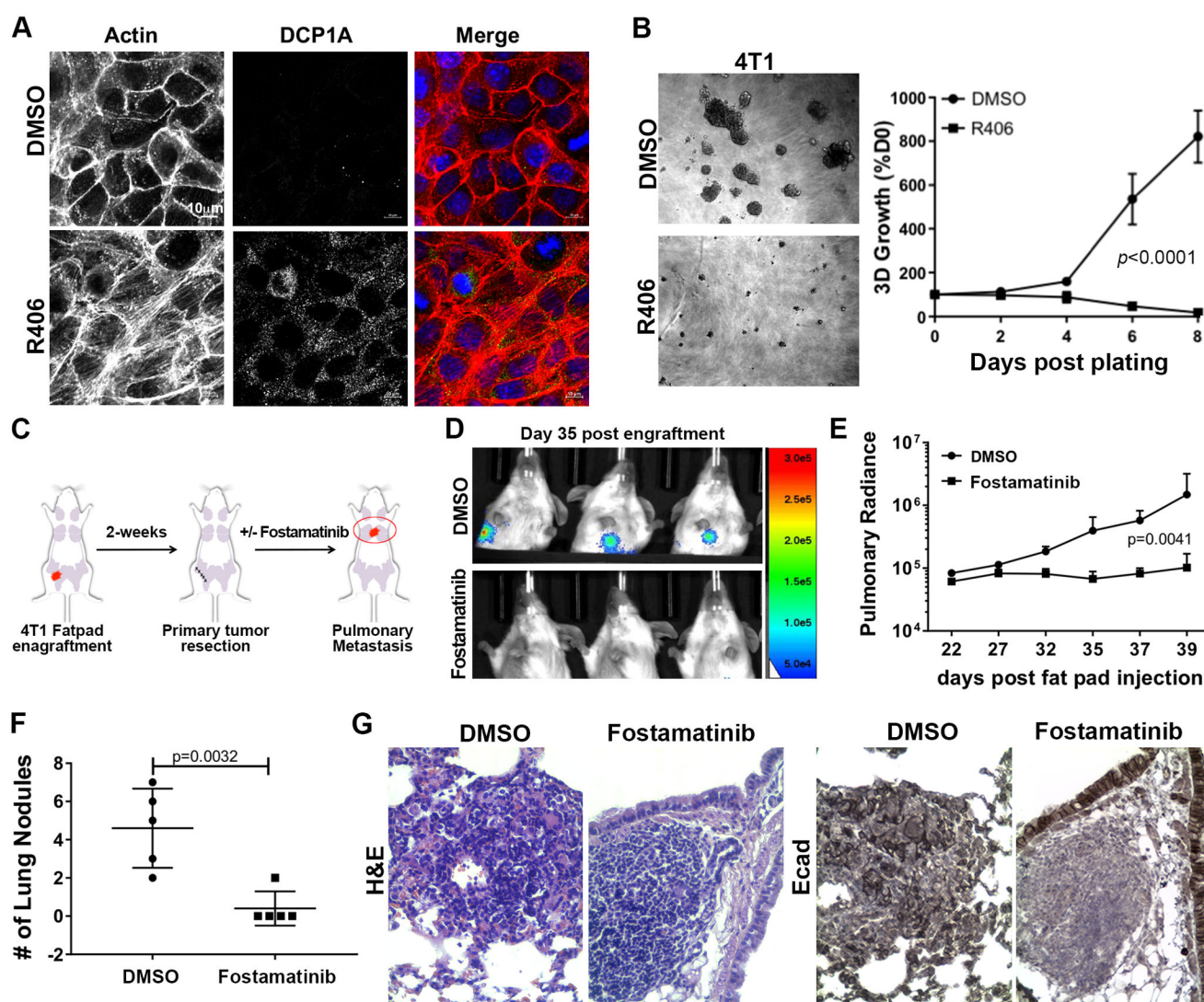


Figure 7. Inhibition of SYK stabilizes a mesenchymal phenotype and inhibits pulmonary metastatic outgrowth.

(A) 4T1 cells were treated with R406 (1 μ M) for 18 days, fixed and stained with phalloidin (red) to visualize redistribution of the actin cytoskeleton and antibodies against DCP1A (green) to visualize P-body formation. Nuclei (blue) were counterstained with DAPI. (B) 4T1 cells were placed under single cell 3D culture conditions in the absence (DMSO) or presence of R406 (1 μ M) and cellular outgrowth within these cultures was quantified by bioluminescence at the indicated time points. Data are the mean \pm SE of two independent assays completed in triplicate, resulting in the indicated P value. (C) Schematic representation of the experimental approach. 4T1 primary tumors were established and surgically resected. Following this procedure mice were treated with fostamatinib (50mg/kg; PO qd). (D) Representative BLI images of mice treated as described in panel C. (E) Pulmonary radiance values for control (DMSO) and fostamatinib treated mice at the indicated time points. (F) Upon necropsy macroscopic pulmonary metastasis were enumerated in lungs of control (DMSO) and fostamatinib treated mice. Data in panels E and

F are the mean \pm SE of five mice per group resulting in the indicated P values. (G) Histological sections of similar sized 4T1-metastases in control (DMSO) and fostamatinib-treated groups. Sections were stained with H&E or antibodies against Ecad.

Author Manuscript

Author Manuscript

Author Manuscript

Author Manuscript